



# Water/ice as sprayable sacrificial materials in low-temperature 3D printing for biomedical applications



Chao-Yang Liao <sup>a,\*</sup>, Wei-Jen Wu <sup>a</sup>, Cheng-Tien Hsieh <sup>b</sup>, Hung-Ching Yang <sup>a</sup>, Ching-Shiow Tseng <sup>a</sup>, Shan-hui Hsu <sup>b,\*</sup>

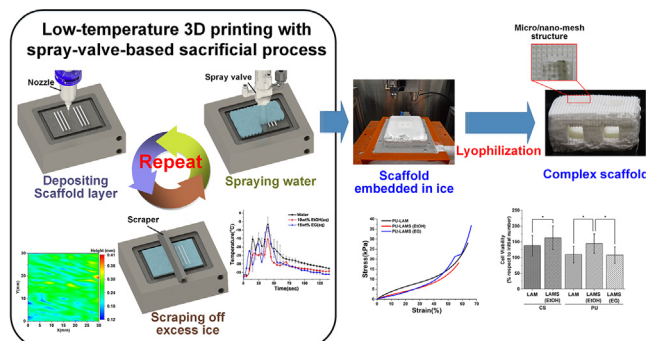
<sup>a</sup> Department of Mechanical Engineering, National Central University, Taoyuan 32001, Taiwan

<sup>b</sup> Institute of Polymer Science and Engineering, National Taiwan University, Taipei 10617, Taiwan

## HIGHLIGHTS

- Water/ice as sprayable support materials for low-temperature 3D printing is developed.
- The sacrificial process utilizes the phase change of water and is suitable for making tissue engineering scaffolds of complex shapes with high porosity.
- The support material is rapidly sprayed on a two-dimensional area and completely removed after scaffold fabrication.
- Addition of some ethanol or ethylene glycol helps water forming creamy ice, a softer support compared to ice.
- The mechanical properties of the printed structures and the cell viability are properly maintained.

## GRAPHICAL ABSTRACT



## ARTICLE INFO

### Article history:

Received 23 August 2018

Received in revised form 5 October 2018

Accepted 6 October 2018

Available online 7 October 2018

### Keywords:

3D printing  
Additive manufacturing  
Tissue engineering  
Sacrificial process  
Support structure  
Low-temperature deposition

## ABSTRACT

A spray-valve-based sacrificial process and “water/ice” support materials were developed in this study, based on the phase changes of water and low-temperature AM technology. The process entails utilizing the three phases of water to effectively and rapidly generate support structures that can also be efficiently removed completely after fabrication. Two scaffold materials, polycaprolactone-based waterborne polyurethane and chitosan, were tested. Moreover, ethanol or ethylene glycol was employed as the additive of pure water for facilitating the removal of excess support materials during fabrication. To verify the proposed sacrificial process, three complex and large scaffolds were fabricated, including a Y-type tubular scaffold, a square scaffold with dual inverted T-type inner channels, and a three-layer tapered scaffold. Results revealed that the properties of the printed complex structures were properly maintained and the adhesion between the layers was firm enough to resist elastic deformation.

© 2018 Elsevier Ltd. This is an open access article under the CC BY-NC-ND license (<http://creativecommons.org/licenses/by-nc-nd/4.0/>).

## 1. Introduction

Tissue engineering (TE) involves the seeding of cells in a three-dimensional (3D) matrix (“scaffold”), which supports cells to migrate, proliferate, differentiate, and eventually gain the function of the target

\* Corresponding authors.

E-mail addresses: [cyliao@ncu.edu.tw](mailto:cyliao@ncu.edu.tw) (C.-Y. Liao), [shhsu@ntu.edu.tw](mailto:shhsu@ntu.edu.tw) (S. Hsu).

tissue. To design a scaffold, microporous structures are of essential importance because they allow the diffusion of nutrients and waste products to and from cells. When scaffolds are implanted, the microporous structures also enable the scaffolds to integrate and to establish vascular anastomosis with natural tissue. Recent research attention has been focused on fabricating TE scaffolds by additive manufacturing (AM) technology, also called 3D printing, which can control the size and number of the pores in scaffolds precisely [1–5], compared with traditional techniques such as solvent casting and fiber spinning [6]. To achieve a biomimetic structure, such as an ear or trachea, AM should be able to produce a shape with either a suspended or hollow tubular structure. Such types of structures produced by AM techniques conventionally need a sacrificial process to make a temporary support layer in order to retain the structures and avoid collapse [7,8].

The low-temperature AM (LAM) is an extrusion-based AM technique. Biomaterials are extruded from the nozzle, deposited under a cryogenic condition through layer-by-layer manufacturing, and lyophilized to become a scaffold. Studies have demonstrated the use of LAM to extrude various biomedical materials in a solvent through a nozzle and to freeze them into scaffolds [9–15]. LAM mainly utilizes the phase transition of a liquid to a solid. Because the environmental temperature is considerably lower than the freezing point of the solvent, the solution freezes rapidly in this technology, resulting in a thermally induced phase separation process [9]. After lyophilization, the solvent is extracted, and the biomedical material remains as the scaffold. The cavities caused by solvent extraction are distributed around the strand surface. Therefore, scaffolds made by LAM can be both macroporous and microporous and can facilitate cell attachment. Microporous surface is one of advantage of using LAM process. In our previous research, we used poly(lactic-co-glycolic acid) (PLGA) to produce scaffolds through traditional fused deposition modeling (FDM) and LAM processes. After the FDM process, the average molecular weight of PLGA decreased to 22.4% of its original value [16]. By contrast, the molecular weight remained unchanged after the LAM process. The reason for this difference is that thermal hydrolysis occurs during the melt-extrusion process, which tends to reduce the structural strength of the scaffolds [17], and this highlights another advantage of LAM. We also made an attempt to avoid the use of organic solvent (1, 4-dioxane) as in the LAM process of PLGA scaffolds by synthesizing waterborne polycaprolactone (PCL)-based polyurethane (PU) [18,19]. The water suspension of PU was mixed with a little poly(ethylene oxide) (PEO) as a viscosity enhance to produce elastic scaffolds through the LAM process [20]. The structure of biodegradable PU comprises soft segments of hydrolyzable PCL; accordingly, PU can be degraded through the hydrolysis of the soft segments [21]. The green synthetic process of biodegradable waterborne PU as well as the organic solvent-free LAM process is ecologically friendly. Meanwhile, studies have applied LAM to other naturally derived polymers such as chitosan (CS) [22] and gelatin [10]. Multiple-material printing was also investigated [23,24]. For example, Liu et al. [25] fabricated composite scaffolds of collagen and PLGA by LAM to simultaneously achieve hydrophilicity and mechanical strength. In nearly all these studies, cells are seeded onto the lyophilized scaffolds for culturing, eventually enabling the cells to adopt the function of the target tissue. In some special case, cell-laden scaffolds were directly fabricated by using LAM without lyophilization [26].

AM coupled with the sacrificial process can produce a hollow structure for TE applications such as vascular networks [27] or tracheae [28] and branching or suspended structures such as noses or ears [29]. Instead of using a sacrificial process, studies also have developed unique approaches to fabricating complex scaffolds [30–34]. Ideally, pure water can be used as the support material in a LAM process. However, in order to reduce the hardness of ice and adjust the freezing points of the support material to meet the main material requirement, previous studies were added specific additives into the water [35,36]. Ethanol (EtOH) or ethylene glycol (EG) can also be added into the pure water. At low temperatures, these aqueous solutions (aqs) appear in the

form of clathrate hydrates, similar to creamy ice, and can be easily removed theoretically. Regarding the sacrificial processes of LAM technology, the support material is also extruded through a nozzle and frozen to form the support structure. After scaffold fabrication, the support structure can be removed from the scaffold by utilizing differences in melting points [35] or applying the burnout method after freeze-drying [36]. However, these methods not only have long processing times but also fail to fully capitalize on the phase change characteristics of materials in LAM.

In this article, we focused on developing an effective method of fabricating complex scaffolds in low-temperature environments. Two scaffold materials were used to verify that a “water/ice” support structure can be employed to fabricate TE scaffolds and that the sacrificial process is nontoxic for cell growth. One of the materials was PCL-based waterborne PU as previously mentioned. The other was CS, a popular biomaterial in TE applications. The effectiveness of our proposed sacrificial material process was validated by producing three complex scaffolds with different shape designs.

## 2. Methods and materials

### 2.1. Sacrificial process utilizing phase changes of water for LAM technology

We devised a frozen-form AM system that can produce a uniform cryogenic environment, as shown in Fig. 1(a) [37]. In this system, a peristaltic pump circulates the coolant around the cooling enclosure (yellow arrows indicating the direction). The working plate is in contact with the cooling enclosure; therefore, it can also be cooled down through conduction. In addition, the working plate can be moved up and down freely within the cooling enclosure. After a layer of scaffold is fabricated, the working plate is lowered by a specific height through the vertical stage, and the system subsequently starts fabricating the next layer. Thus, with respect to the cooling area, the deposition level of the materials can remain unchanged and certain degrees of consistency in temperature distribution exist across areas of the same height.

In this study, taking advantages of the low-temperature freezing, we developed a scaffold fabrication procedure involving a spray-valve-based sacrificial process (hereinafter referred to as LAMS process) by adopting water/ice as the support material (Fig. 1(b)). The main concept of the proposed sacrificial process is to take water as the fed support material and nebulize it with a spray valve on top of the scaffold and in its vicinity. Because of the cryogenic environment, the water is frozen to support the upper structure. During the lyophilization process, ice is sublimed from the main body of the scaffold, and the final scaffold is consequently obtained.

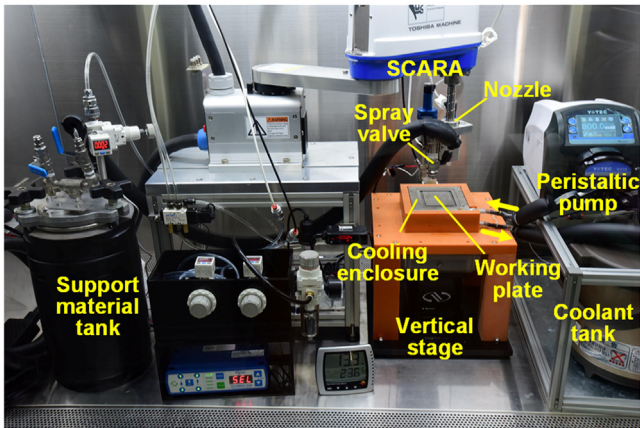
In the spraying process, water fully covers the top layer of the scaffold. After the water has been frozen, a designed scraper is used to scrape the excess ice. Before the scraper is used, the working plate descends within a small specific distance in advance. Therefore, during removal of the excess ice by the scraper, the topmost layer of the strands of scaffold would be touched. Because the strands are firmly embedded in the ice, they would not be scraped off.

By employing a spray valve in a 2D operating mode to nebulize materials in a large region, the efficiency of AM can be increased. However, precise control for the location of material deposition by a spray valve is rather difficult. For this reason, studies in the field of AM have mainly focused on fast interior filling [38]. The support structure does not considerably affect the accuracy of the scaffold, but it does substantially affect the building time. Therefore, in the current study, a spray valve was used to accelerate the generation of the support layer (ice).

### 2.2. Materials and their preparations

Waterborne biodegradable PU was synthesized by mixing a soft segment of PCL diol ( $M_n = 2000$  g/mol; Sigma-Aldrich, USA) and polyethylene butylene adipate diol ( $M_n = 2000$  g/mol; Greco, Taiwan) in a

(a)



(b)

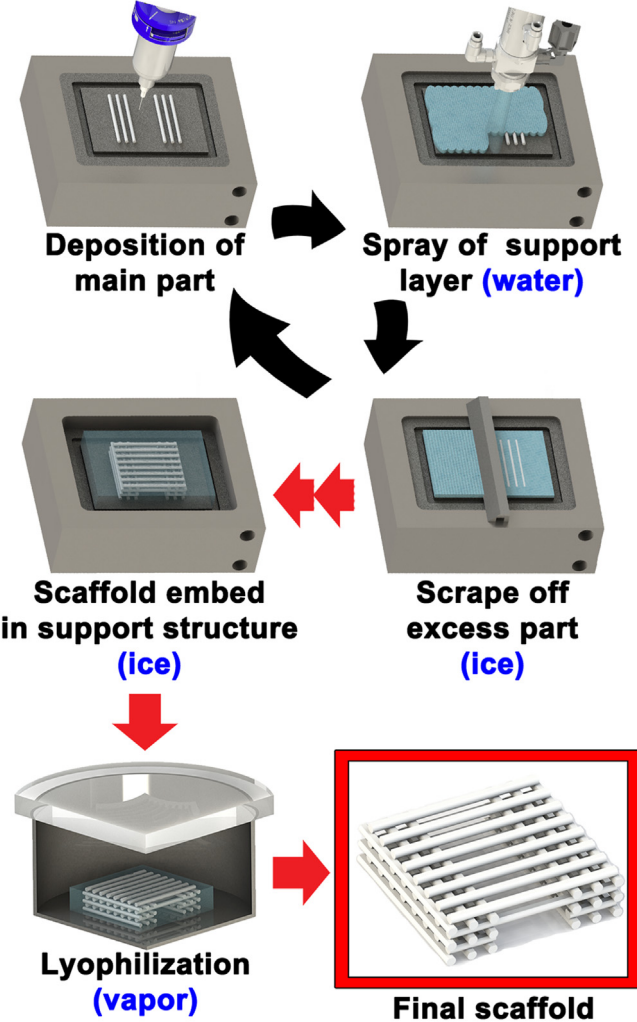


**Fig. 1.** Schematics of the sacrificial process utilizing phase changes of water for LAM, as well as the experimental equipment: (a) Frozen-form AM system developed by our team (total build volume = 75 mm × 50 mm × 21.6 mm). (b) Scaffold fabrication with the proposed sacrificial process.

2:3 M ratio. The hard segment comprised isophorone diisocyanate (IPDI; Evonik Degussa, Germany) and two chain extenders, namely 2, 2-bis(hydroxymethyl) propionic acid (DMPA; Sigma-Aldrich, USA) and ethylenediamine (EDA; Tedia, USA). The molar feed ratio of IPDI/oligodiols/DMPA/EDA was 3.52:1:1:1.52. The molecular structure

could be tuned to obtain various PU materials with different degradation rates and elasticities. The solid content of PU aqueous dispersion was adjusted to approximately 30 wt%. Poly(ethylene oxide) (PEO, Mw = 900 kDa; Scientific Polymer Products, USA) was dissolved in deionized (DI) water to prepare 10% (w/v) PEO solution at 60 °C under magnetic stirring. The PU ink was prepared by mixing the PEO solution with PU dispersion for 24 h at a mass ratio of 74/26. Additional details can be found in the report of our previous work [18]. CS (viscosity: 0.2–0.4 Pa·s) was obtained from Sigma-Aldrich (USA). In total, 2.5 g of CS was dissolved in 97.5 g of 1% (v/v) acetic acid (aq) until a homogeneous 2.5 wt% CS solution was obtained, serving as the CS ink. Anhydrous EtOH and EG were acquired from ECHO (Taiwan).

### 2.3. Measuring freezing points of scaffold materials

The eutectic temperature was measured using a differential scanning calorimeter (TA Q-20, USA). The temperature of the PU ink was lowered to –20 °C at a rate of 20 °C min<sup>–1</sup>, maintained at –20 °C for 5 min, and then increased to 10 °C at a rate of 0.25 °C min<sup>–1</sup>. The temperature of the CS ink was lowered to –60 °C at a rate of 20 °C min<sup>–1</sup>, maintained at –60 °C for 5 min, and then increased to 10 °C at a rate of 0.25 °C min<sup>–1</sup>. The freezing point of the PU ink was determined by its eutectic temperature. However, the eutectic temperature of the CS ink could not be determined by the differential scanning calorimeter. Therefore, the freezing point of the CS ink was determined visually. Specifically, the CS ink was deposited on the working plate at 10 °C, and the temperature was lowered at a rate of –1.67 °C min<sup>–1</sup>. The temperature at which the CS ink fully transformed into a solid state was recorded as the freezing point of the ink.

### 2.4. Scaffold fabrication

An air-powered fluid dispenser (Nordson EFD Ultimus V, USA) with a nozzle (0.2 mm in diameter) was used to extrude the scaffold material, and a spray valve (Nordson EFD 781S—46F, USA) was used to spray support materials. Both were mounted on the end arm of a selective compliance assembly robot arm (SCARA; Toshiba THL400, Japan). The SCARA has a light structure and quick response, and thus is suitable for planar positioning and pick-and-place tasks for professional assembly operations. Additionally, a dehumidifier (Munters M120, Sweden) was used to decrease the humidity of surrounding environment in order to avoid the frost which may affect the interlayer adhesion.

Fig. 2 shows five scaffolds of varying sizes and appearances. Fig. 2 (a) and (b) presents cylindrical scaffolds with a 6.5-mm diameter. The cylindrical scaffold in Fig. 2(a) was measured 4.8 mm in height, which comprised sequentially arranged every two layers stacked at angles of 0°, 45°, 90°, and 135° for mechanical property measurement and cell viability assay. To facilitate the process of capturing fluorescent images, the height of the scaffold in fig. F(b) was only 0.8 mm, and this scaffold comprised sequentially arranged layers stacked at angles of 0°, 45°, 90°, and 135°.

To verify that the proposed LAMS process can be employed to fabricate complex and hollow structures, a Y-type tubular scaffold (4.4 mm in diameter, 3.2 mm in inner diameter, 20 mm in length), a large square scaffold (30 mm × 30 mm × 15 mm) with two inverted T-type inner channels, and a three-layer tapered scaffold (20 mm × 20 mm on the larger end and 10 mm × 10 mm on the smaller end, with each taper measuring 4 mm in height) were produced. The Y-type tubular scaffold had a smooth enclosed surface to simulate the blood vessel, and the corresponding dimensions are shown in Fig. 2(c). For the square scaffold, the dimensions of the main structure and a cross-sectional view of one of the inverted T-type inner channels are illustrated in Fig. 2(d). The front of the scaffold had two square holes passing through the channels. The top of the scaffold also had two rectangular holes connecting to the aforementioned channels. Apart from the channel space, the other parts of this scaffold were composed of pore structures. For the three-

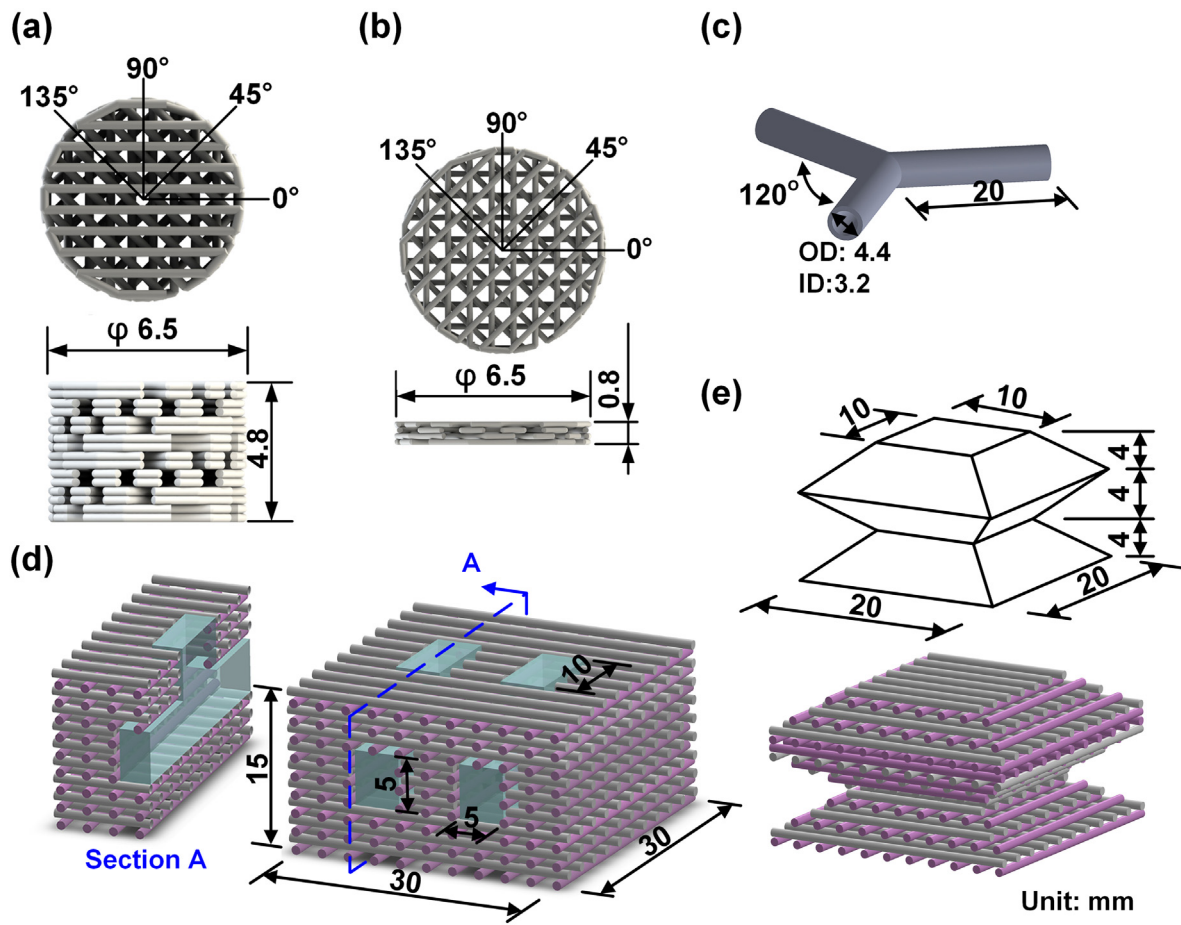


**Fig. 2.** Scaffolds fabricated in this study: (a) and (b) cylindrical scaffold; (c) Y-type tubular scaffold; (d) square scaffold with dual inverted T-type inner channels; and (e) three-layer tapered scaffold. For better illustration, (d) and (e) are shown as schematic diagrams.

layer tapered scaffold, four inclined planes intersected the horizontal plane at 21.8° (shown in Fig. 2(e), along with the corresponding dimensions).

When the temperature of the working plate dropped to a predefined temperature, the scaffold was fabricated from the nozzle at a SCARA moving speed of 12.67 mm s<sup>-1</sup>. For scaffolds fabricated only with the LAM process, the working plate dropped one layer thickness after the fabrication of a scaffold layer, and the next scaffold layer was subsequently fabricated at the level of the previous layer through material deposition. After fabrication, the scaffold were lyophilized (SP Scientific VirTis BenchTop Pro, USA).

For scaffolds fabricated with the LAMS process, the procedures of extruding scaffold materials and spraying support materials were performed alternately. Table 1 presents the essential manufacturing parameters for cylindrical scaffold fabrication. By using different

scaffold materials and support materials, and applying or not applying a sacrificial process, we developed five manufacturing combinations for the cylindrical scaffolds.

The Y-type tubular scaffold and the large square scaffold with two inverted T-type inner channels were fabricated by the LAMS process, with PU and 10 wt% EtOH (aq) as the scaffold and support materials, respectively. The manufacturing parameters were based on those presented in Table 1, except that the spraying pressure for the support material was reduced to 400 kPa, the strand diameter was reduced to 0.2 mm, the layer thickness was reduced to 0.2 mm, and the pore size was increased to 0.8 mm. The three-layer tapered scaffold was also successfully fabricated by the LAMS process, using CS and 10 wt% EtOH (aq) as the scaffold and support materials, respectively. Except for the pore size, which was changed to 0.7 mm, the manufacturing parameters were mainly the same as those presented in Table 1.

**Table 1**  
Manufacturing parameters for PU and CS cylindrical scaffolds by LAM and LAMS processes.

Scaffold material	Scaffold viscosity (Pa·s)	Process	Support material (aq)	Pressure (kPa)		Temperature of working plate (°C)		Scanning velocity (mm s <sup>-1</sup> )		Nozzle diameter (mm)	Predefined strand diameter (mm)	Pore size (mm)	Layer thickness (mm)
				Scaffold	Support	Scaffold	Support	Scaffold	Support				
PU	2.794	LAM	–	175	450	−30		12.67	36.67	0.2	0.3	0.4	0.3
		LAMS	10 wt% EtOH	175		−30							0.3
	1.327	LAMS	15 wt% EG	175		−40							0.3
CS	1.327	LAM	–	65		−30							0.2
		LAMS	10 wt% EtOH	65		−30							0.2

## 2.5. Measuring the temperature of the working plate for spraying support materials

When the temperature of the working plate dropped to a predefined temperature (i.e., by  $-37^{\circ}\text{C}$ ), the spray valve sprayed the appropriate support material 10 times by alternating left and right as well as back and forth at a SCARA moving speed of  $36.67\text{ mm s}^{-1}$  to complete a support layer. To obtain favorable results, the thickness of the frozen layer must be slightly greater than the predefined layer thickness (i.e., by 0.2 mm). Accordingly, when the temperature of the working plate returned to the predefined temperature, the working plate was lowered in accordance with the predefined layer thickness, and the excess support materials were manually removed with a scraper. Subsequently, the next layer was sprayed.

Before the fifth layer was sprayed, a thermal imaging camera (FLIR A615, USA) was turned on and the lenses were aligned to the center of the working plate to capture a reading every 5 s, recording the temperature changes in the process of spraying support materials. Pure water, 10 wt% EtOH (aq), and 15 wt% EG (aq) were tested as the support materials in the experiments. Each experiment was repeated three times, and the mean value and a standard deviation were derived for the measured quantities.

## 2.6. Measurement of the deposited layer height on the working plate

A charge-coupled device (CCD) laser displacement sensor (Keyence LK-G85A, Japan) was used to measure changes in the deposition plane of the working plate. The laser sensor and nozzle were placed on the end arm of the SCARA. The sampling frequency of the sensor was set to 2 ms. The moving speed of the SCARA was  $12.5\text{ mm s}^{-1}$ . The scan area was  $45\text{ mm} \times 60\text{ mm}$ , and scans were performed every 3 mm and in a zig-zag motion beginning from the  $x$ -axis and moving along the  $y$ -axis. Along each  $y$ -axis scan line, one point was taken every 1 mm, obtaining a total of 960 points that were used to create a contour map of the scan area.

When the temperature of the working plate reached  $-30^{\circ}\text{C}$ , the nozzle squeezed out the PU ink and deposited it on the working plate. A total of 11 strands were fabricated. Each strand was 20 mm in length and approximately 0.2 mm in height, with the distance between strands being 2 mm. Subsequently, the area was scanned using the laser sensor to obtain a contour map of the deposition plane. Next, 10 wt% EtOH (aq) was sprayed on the working plate. The thickness of the frozen layer was approximately 0.3 mm. The laser sensor was again used to acquire the scan area. The working plate was then lowered by 0.2 mm and the excess support materials were removed using the scraper, after which the deposition plane was scanned. Finally, the second layer of PU ink was squeezed using the nozzle on the deposition plane, after which the deposition plane was scanned again.

## 2.7. Mechanical properties of scaffolds and support materials

The static and dynamic compression behaviors of the cylindrical scaffold (Fig. 2(a)) immersed in phosphate buffered saline (PBS) were evaluated using a dynamic mechanical analyzer (TA Q-800, USA). The dynamic compression test was performed using a strain of 0.1% and preload of 2 mN at a frequency of 1 Hz at  $37^{\circ}\text{C}$ . The static compression test was performed using a preload of 0.01 N at  $37^{\circ}\text{C}$ . The machine was controlled at a speed of  $2\text{ N min}^{-1}$ ; subsequently, the loads and the corresponding compressive strains were recorded. When the load reached 18 N, the machine stopped recording.

The hardness of the frozen support materials was tested using a Shore durometer (Bareiss HPE III, Germany). The support materials were sprayed on top of the working plate to deposit a support layer with a thickness of 6 mm. The scraper was used to remove uneven parts of the support layer. When the temperatures of the working

plate were at  $-10$ ,  $-20$ ,  $-30$ , and  $-40^{\circ}\text{C}$ , the durometer measured the hardness at the center and four corners of the support layer surface.

## 2.8. Cell culture

Human-induced pluripotent stem (iPS) cell-derived mesenchymal stem cells (MSCs) were generated from human umbilical vein endothelial cells (Bioresource Collection and Research Center, Hsinchu, Taiwan) transfected with Oct 4 and Sox 2 by lentivirus and subsequently differentiated into MSCs by switching from iPS medium to MSC medium [39,40]. The MSCs were cultured in Dulbecco's modified Eagle's medium-low glucose; the medium was supplemented with  $3.7\text{ g L}^{-1}$  sodium bicarbonate, 1% penicillin-streptomycin, 1% L-glutamine, and 10% fetal bovine serum. All MSCs were incubated in 5%  $\text{CO}_2$  at  $37^{\circ}\text{C}$ , and the medium was refreshed twice every week.

## 2.9. Cell viability assay

The dimensions of the scaffolds used for measuring cell viability are illustrated in Fig. 2(a). Before the experiment, the scaffolds were sterilized with ultraviolet light for 6 h. After being washed with PBS, the scaffolds were placed in a six-well tissue culture plate. The MSC suspension (volume:  $10\text{ }\mu\text{L}$ ) containing  $10^6$  cells was seeded onto the top center of the scaffold surface. The culture plate was moved and incubated in 5%  $\text{CO}_2$  at  $37^{\circ}\text{C}$  for 3 h. Subsequently, the culture medium was added for 24 h of cultivation. Cell viability was measured through the MTT assay. A tetrazolium dye (Sigma-Aldrich, USA) was used to react with the MSCs at  $37^{\circ}\text{C}$  in a dark environment for 4 h. Next, the tetrazolium dye was removed and  $300\text{ }\mu\text{L}$  of anhydrous EtOH was then added to dissolve the formazan crystals. Finally, a microplate reader (SpectraMax M5, USA) was used to measure the optical density of the crystal-dissolving solutions at an absorption wavelength of 570 nm.

## 2.10. Cell labeling

The scaffolds for cell labeling were produced as cylinders measuring 6.5 mm in diameter and 0.8 mm in height (Fig. 2(b)). The MSCs were labeled with a fluorescent dye (PKH26, Sigma-Aldrich, USA) in vitro. The cells (density:  $10^7\text{ cells mL}^{-1}$ ) were labeled by mixing with  $2 \times 10^{-6}\text{ M}$  PKH26, which can be stably incorporated into the cell membrane because of its long aliphatic tails. The labeling process was stopped by adding complete medium. The labeled cells were washed with PBS and then seeded onto the top center of the scaffold surface by using same preparation method as described at Section 2.9. The final cell density in the scaffold was  $10^6$  cells per scaffold. After 24 h, the cells were observed under a fluorescence microscope.

## 2.11. Surface morphology

The morphology of scaffolds was investigated under a scanning electron microscope (SEM; JEOL JSM-7000F, Japan). The samples were dried under vacuum at room temperature overnight, followed by platinum coating.

## 3. Results and discussion

### 3.1. Selection of support materials for the proposed sacrificial process

For fabrication of a complex scaffold, emphasis is placed on not damaging the scaffold and on the ability to completely remove the support materials, as well as on the nontoxicity of the fabrication process. Accordingly, we first used pure water as the support material and then performed the testing procedures. The freezing point of pure water is  $0^{\circ}\text{C}$ , with a latent heat of melting of  $334\text{ J g}^{-1}$ . In general, the temperature of the working plate of a LAM system is maintained at

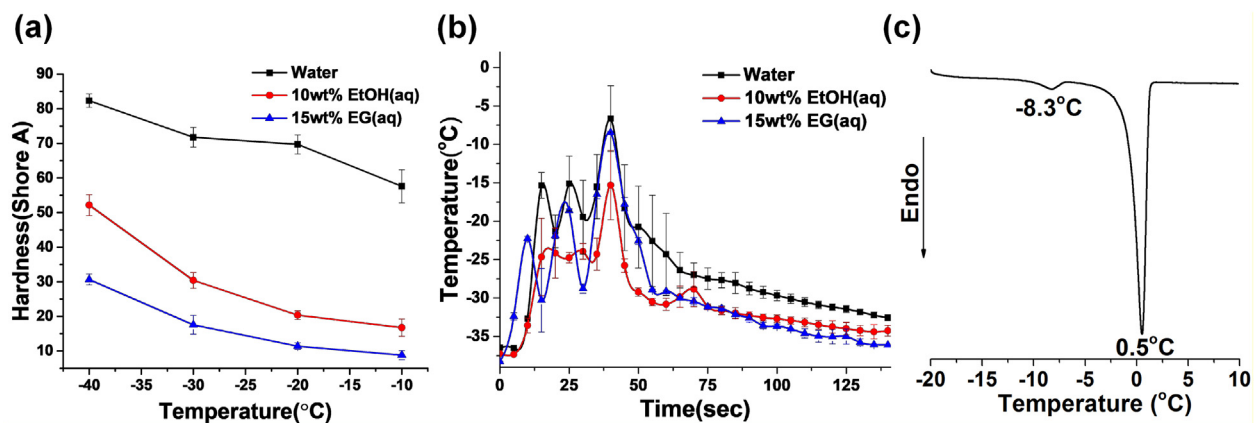


**Fig. 3.** Characteristics of support and scaffold materials in a low-temperature environment. (a) Hardness scale of support materials in a Shore durometer (type A). (b) Temperature measurement for the process of spraying support materials on the working plate. (c) Eutectic temperature measurement of PU ink by a differential scanning calorimeter.

–20 to –40 °C. Thus, when pure water is used as the support material to be sprayed on the working plate and the scaffold, it can freeze rapidly.

The hardness scale of ice in a Shore durometer (type A) was determined to range from  $57.6 \pm 4.8$  to  $82.3 \pm 2.0$  at –10 to –40 °C (Fig. 3(a)). Therefore, scraping off the excess ice from the firm support layer by a scraper would be detrimental. In Fig. 3(b), the black line indicates the temperature variation of a single support layer constructed using a spray valve. For a single support layer, the total spraying time was 35 s, with the corresponding thickness of 0.2–0.3 mm. In only 125 s, a support layer was firm enough for the scraping process.

Because of the release of the latent heat of water, the surface temperature of the support layer could increase to a maximum point of  $-6.7 \pm 4.3$  °C, which is even higher than the freezing point of the PU ink (approximately –8.3 °C; Fig. 3(c)) and is near that of the CS ink (approximately –6.8 °C). At this point, the PU scaffold surface could be partially dissolved. As noted, the eutectic temperature of CS ink (~–6.8 °C) could not be detected by the differential scanning calorimeter. Therefore, the freezing point of the CS ink was determined through visual observation in this study.

Accordingly, a small amount of EtOH was added to the pure water to reduce its latent heat. At room temperature, EtOH is highly volatile to facilitate complete removal after scaffold fabrication; in particular, its latent heat of  $108 \text{ J g}^{-1}$  is much lower than that of water. As reported by the Seager et al. [41,42], a solution with an EtOH content of less than 10 wt% is more appropriate for use with a commercially available lyophilizer.

If water contains a low EtOH content, it is first crystallized (ice) before being cooled to the eutectic temperature. The remaining solution can be continuously concentrated until all of the water has been crystallized, and clathrate hydrate II ( $\text{EtOH} \cdot 17\text{H}_2\text{O}$ ) is thus formed [43]. This clathrate is a solid clathrate compound in which numerous EtOH molecules are trapped within the crystal structure of water, forming a solid with a similar appearance to creamy ice. Based on experimental data, the hardness scale of  $\text{EtOH} \cdot 17\text{H}_2\text{O}$  converted from the 10 wt% EtOH (aq) ranged from  $16.7 \pm 2.5$  to  $52.1 \pm 3.0$  at –10 to –40 °C in the Shore durometer (type A) (Fig. 3(a)). Therefore, the hardness scale was 37%–71% lower than the ice. Such creamy characteristics of the EtOH clathrate is conducive to the proposed sacrificial process because the excess support material can be scraped off easily without damaging the scaffold beneath it.

Regardless of whether ice or clathrate hydrate II is used, if the spaces between the water molecules within the solid-state structure increase after solidification, the density would decrease and the volume would increase. According to our experiment, the density of 10 wt% EtOH (aq) after solidification was  $0.94 \text{ g cm}^{-3}$ , whereas the density of its liquid form at 20 °C was  $0.98 \text{ g cm}^{-3}$  [44], and the volume expanded by approximately 4.3%. In contrast, the volume of pure water expands by

nearly 8.7% under the same conditions. Hence, the volume expansion was smaller for water with 10 wt% EtOH (aq). To reduce the latent heat and hardness of the support material and to reduce the volume change caused by the phase change, we mainly used 10 wt% EtOH (aq) as the support material in this study. As shown in Fig. 3(b), when 10 wt% EtOH (aq) (red line) was sprayed on the working plate to construct a single support layer, the highest temperature reached was only  $-15.3 \pm 4.5$  °C, which is well below the freezing points of the PU and CS scaffolds.

EtOH is a common solvent that may partially dissolve PU and CS during a slow freeze-drying process, forming a mesh structure around the scaffolds (as discussed in Section 3.3). For comparison with the results obtained using 10 wt% EtOH (aq), we also employed 15 wt% EG (aq) (in which PU does not dissolve) as the second support material. The latent heat of EG is  $181 \text{ J g}^{-1}$  and also lower than that of pure water. As shown in Fig. 3(b), when 15 wt% EG (aq) (blue line) was sprayed on the working plate to construct a single support layer, the highest temperature reached was  $-8.5 \pm 0.2$  °C. The temperature was slightly lower than that using pure water (~–6.7 °C) but relatively higher than that using 10 wt% EtOH (aq) (~–15.3 °C). Furthermore, the maximum temperature range of 15 wt% EG (aq) was close to the freezing point of the PU ink, signifying that it may partially dissolve the surfaces of PU scaffolds during spraying. Subsequently, the temperature changes of the working plane were analyzed. The results indicated that during the spraying process, the temperature of the working plane was higher than the PU freezing point for only approximately 0.68 s; considering this finding, in addition to the fact that higher concentrations of EG all failed to meet the basic requirements during the experiments, 15 wt% was selected as the EG concentration.

When being solidified at a temperature of –10 to –40 °C, 15 wt% EG (aq) transformed into a clathrate hydrate and exhibited a hardness scale (measured in the Shore durometer (type A)) of  $8.8 \pm 1.3$  to  $30.7 \pm 1.6$  (Fig. 3(a)), which was lower than that of pure water and EtOH 10 wt% (aq). Therefore, removing the excess ice of 15 wt% EG by the scraper was much easier than removing that of the other two substances. Unlike EtOH, EG could not completely volatilize from the main scaffold structure during the freeze-drying process; rather, EG was mostly condensed in the condensation chamber, with some retained on the scaffold surface. Therefore, the scaffolds were immersed in PBS to remove the EG compound from the scaffolds completely. Because CS can dissolve in EG, the CS ink was not included in the experiment where 15 wt% EG (aq) was adopted as the support material.

### 3.2. Mechanism of support layer accumulation

The key to successfully and rapidly generate a support layer by the spraying method relies on the generation of a flat support layer through

the phase change of the support material, which facilitates the deposition and subsequent layer-by-layer stacking of scaffold materials. Because the support material used in this study was primarily composed of water, which expands when solidified, a curved surface was produced after spraying. To solve this problem, a scraper was designed to remove excess ice without damaging the lower-layer scaffold structure.

**Fig. 4(a)** shows a scheme of the process for removing the excess parts of the support structure by the scraper. When the support material solidified at low temperatures, the sharp surface of the scraper was used to manually and repeatedly remove the excess parts of the support structure. Because the second part of the scraper is a flat surface, the topmost layer strands would be flattened by the scraping motion; thus, the contact area with the top layer strands can be increased, thereby improving the adhesion between layers.

To understand the layer-by-layer stacking situation of the support structure, a CCD laser displacement sensor was employed to measure the height of layers deposited on the working plate at various stages. **Fig. 4(b)** depicts an image of the heights of the first scaffold layer deposited on the working plate. To produce the best image, only the region surrounding the scaffold (measuring approximately  $30 \text{ mm} \times 30 \text{ mm}$ ) is depicted. The image reveals an average layer height of  $0.03 \pm 0.06 \text{ mm}$ . Because the height of a scaffold layer is around  $0.2 \text{ mm}$ ; to ensure that the entire scaffold space was filled, the support material was sprayed, creating a single-layer height of approximately  $0.3 \text{ mm}$  after solidification. As indicated in **Fig. 4(c)**, the deposition plane exhibited an irregular wave surface and an average layer height of  $0.28 \pm 0.13 \text{ mm}$ .

Next, the working plate was lowered and the scraper was used repeatedly to remove the excess parts of the support structure. **Fig. 4(d)** shows that the irregular wave surface became flat again. In addition, because the top of the scaffold strands were flattened by the flat surface of the scraper, they could not be observed in this figure. Moreover, because the strands were not removed by the scraper, they could be successfully embedded into the support layer, which had an average height of  $0.23 \pm 0.03 \text{ mm}$ , as indicated in the figure. The second scaffold layer was again deposited, which had an average height of  $0.24 \pm 0.07 \text{ mm}$ .

**Fig. 4(e)** shows a scheme of the process of scraping off excess parts of the support structure by a designed scraper. These results reveal that the scraper can effectively produce a flat deposition surface for the subsequent deposition of scaffold materials.

### 3.3. Comparison in surface morphology of the scaffolds between LAM and LAMS processes

After the LAMS process, the unfinished scaffolds were embedded in ice containing specific additives. We adopted the lyophilization process to sublime ice crystals in the scaffold strands to produce the finished scaffolds. The scaffolds were exposed to a vacuum, low-temperature environment during the lyophilization process; therefore, the additive concentrations increased after ice crystal sublimation. The additives were in contact with the surfaces of the scaffold strands for a period of time and may interact with the strands, leading to changes in the properties of the scaffolds.

Scaffolds fabricated using the LAM process differed in morphology from those fabricated using the LAMS process. Concerning scaffolds made using the PU ink, **Fig. 5(a)** and (c) illustrate cylindrical scaffolds fabricated through the LAM and LAMS ( $\text{EtOH}$ ) processes. **Fig. 5(b)** shows the front view of the PU-LAM scaffold for observing the status of layer fusion. The right panel of **Fig. 5(a)** depicts an SEM image of the PU-LAM scaffold, indicating highly clean spaces between the strands and the pores. However, in the PU-LAMS ( $\text{EtOH}$ ) scaffold, both the strands and pores appeared to be in a micro- or nano-mesh structure after lyophilization. The upper-rightest panel of **Fig. 5(c)** presents a magnified view of a portion of the SEM image shown in the middle panel. We suspected that a small portion of water molecules and  $\text{EtOH}$  molecules may penetrate into the PU scaffold, causing slight swelling before the formation of the  $\text{EtOH}$  hydrate [42].

PEO was dissolved in both water and  $\text{EtOH}$ . Although the experiments were conducted at low temperatures, we observed some PEO dissolution from the strands of the PU scaffold. A possible explanation for this observation is that during the lyophilization process, once the water molecules inside the  $\text{EtOH}$  hydrate had sublimed, the  $\text{EtOH}$  molecules escaped from the hexakaidecahedral cages and evaporated

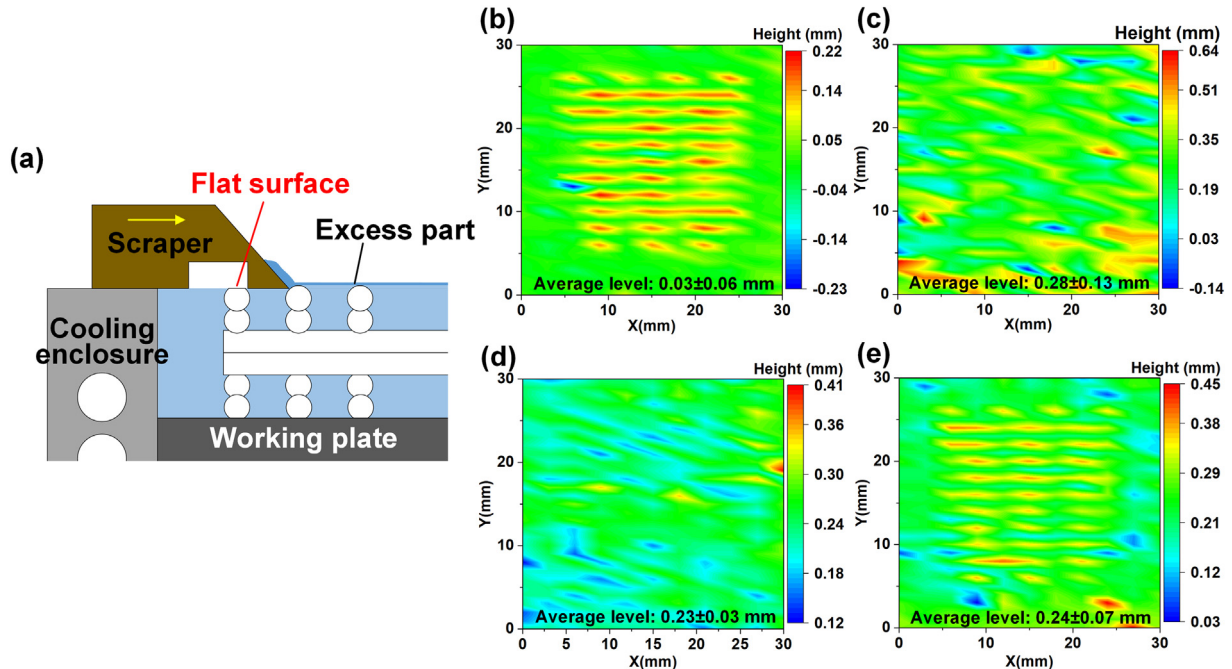


**Fig. 4.** Rapid generation of full-fill and flat support layer. (a) Schematic of the process of scraping off excess parts of the support structure by a designed scraper. (b)–(e) The height of deposited layer on the working plate, as measured by a CCD laser displacement sensor: (b) the first layer deposited for the scaffold; (c) support material sprayed and transformed to be the firm structure; (d) excess parts removed by the scraper; and (e) the second layer deposited for the scaffold.

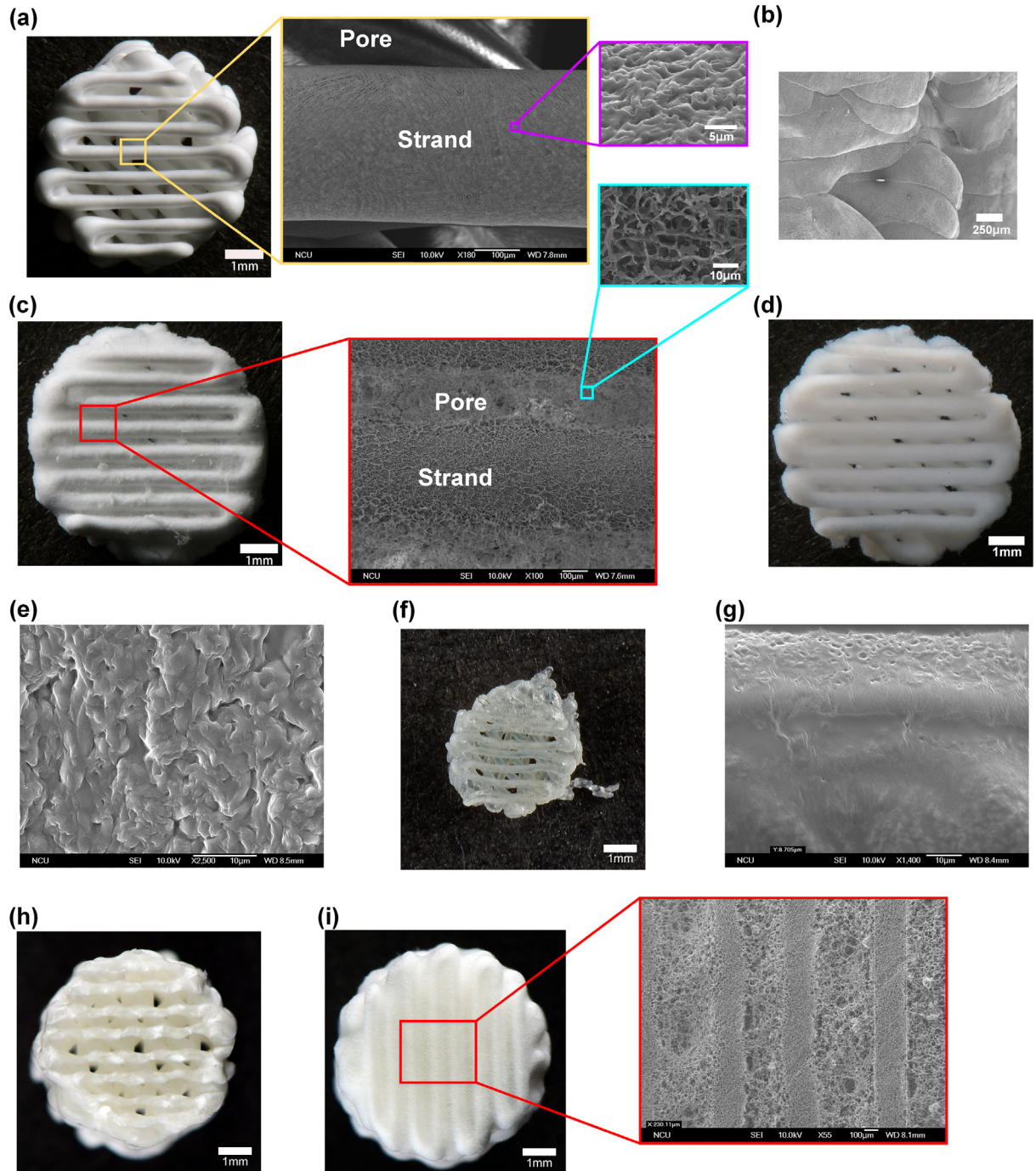


**Fig. 5.** Surface morphology of scaffolds fabricated using LAM and LAMS processes: (a) PU-LAM scaffold; the SEM image in the middle panel is a magnified view of the box in the left panel; the SEM image in the right panel is a magnified view of the box in the image in the middle panel. (b) Front view of the PU-LAM scaffold shown in Fig. 5(a). (c) PU-LAMS (EtOH) scaffold; the SEM image in the upper-right panel is a magnified view of the box in the image in the middle panel. (d) Image obtained after the PU-LAMS (EtOH) scaffold was dipped in DI water and air dried. (e) Magnified view of the strand of the PU-LAMS (EtOH) scaffold shown in Fig. 5(d). (f) PU-LAMS (EG) scaffold. (g) Magnified view of the strand of the PU-LAMS (EG) scaffold shown in Fig. 5(f). (h) CS-LAM scaffold. (i) CS-LAMS scaffold; the image in the right panel is a magnified view of the box in the image in the left panel.

directly because of the extremely low saturated vapor pressure of EtOH in the vacuum; thus, the PEO reticular structure remained. Before cell seeding, the PU scaffold could be dipped in deionized (DI) water to remove PEO. Consequently, we found that after the PU-LAMS (EtOH) scaffold was dipped in DI water, the rough mesh structure disappeared and the clean surface was restored (Fig. 5(d)). This can be ascribed to the redissolution of PEO previously swollen by the support material.

As demonstrated, a small amount of highly volatile EtOH in water can completely evaporate during the lyophilization process. Despite

the presence of any residue, EtOH can be eluted by DI water through immersion without affecting the surface characteristics of the original scaffold or the cell behavior. After the PU-LAM and PU-LAMS (EtOH) scaffolds were dipped in DI water and air dried, they exhibited high similarity in surface morphology (see the rightmost SEM image of Fig. 5(a) and (e)).

Fig. 5(f) shows the PU scaffold fabricated using the LAMS (EG) process. Although PEO did not dissolve in EG, the scaffold did shrink in size, and the adhesion between the scaffold layers was poorer than

that observed for the PU-LAM and PU-LAMS (EtOH) scaffolds. The PU-LAMS (EG) scaffold also changed the color from white to translucent after lyophilization. The SEM image of the strand surfaces of the PU-LAMS (EG) scaffold (Fig. 5(g)) reveals relatively smooth surfaces; the large amount of tiny cavities in the other two scaffolds that were produced after ice crystal sublimation were not observed.

During the LAMS (EG) process, the temperature of the working plate was set at  $-40^{\circ}\text{C}$  to increase the hardness of support structure for scraping. However, small ice crystals were engendered in the scaffold when the PU ink froze. After lyophilization, they formed a small amount of cavities only on the surfaces of the scaffold, which may increase the residual stress on the scaffold and cause the shrinkage and translucent color of the scaffold. Nevertheless, immersion of the scaffold in PBS could induce the water to penetrate into the cavities, thus scattering the light and restoring the original white color of the scaffold. The smoothness of the scaffold and small contact areas between upper and lower strands reduced the adhesion level; therefore, the strands did not well adhere to each other.

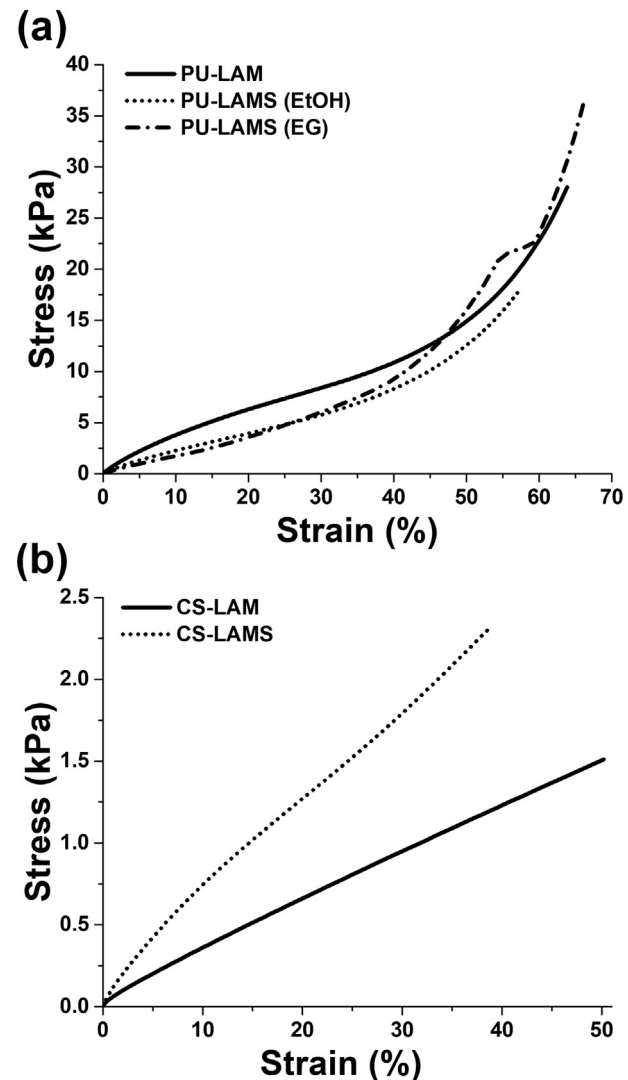
Concerning scaffolds fabricated from the CS ink, Fig. 5(h) and (i) depict the CS-LAM and CS-LAMS scaffolds. Similar to the PU-LAMS (EtOH) scaffold, the pores of the CS-LAMS scaffold had a mesh structure, and the mesh was even denser than that observed in the PU-LAMS scaffold (Fig. 5(i), right panel SEM image). After immersion in DI water, the mesh structure of the CS-LAMS scaffold did not dissolve, which is inconsistent with the phenomenon observed for the PU-LAMS (EtOH) scaffold. A possible reason for this inconsistency is that the CS ink produces a gel when mixed with high-concentration EtOH (aq). Therefore, we surmised that during the freeze-drying process, the gradual increase in EtOH concentration led to gelation of CS on the scaffold surface. Subsequently, as ice crystals were sublimed, the gel may escape from the surface of the strands and gradually enter the inter-strand region, forming a mesh structure with highly concentrated pores.

Table 2 shows the strand diameters (measured from SEM images) of cylindrical scaffolds fabricated using the five manufacturing combinations that are displayed in Table 1. Relative to those of the PU-LAM scaffolds, the strand diameters of the PU-LAMS (EtOH) scaffold were greater by 12.6%. The LAMS (EtOH) process led to the dissolution of PEO from the original scaffold, thereby enhancing the swelling. In contrast, the strand diameters of the PU-LAMS (EG) scaffold were decreased by 30.3% because of increases in internal residual stress. To reduce the swelling phenomenon of scaffolds in the LAMS process in the future, PEO can be replaced with a material that is less readily dissolved in water, such as gelatin [19].

Compared to the CS-LAM scaffold, the strand diameter of the CS-LAMS scaffold was decreased by 23.9%. This could be attributed to the substantial amount of CS gelated and escaping to the inter-strand region.

#### 3.4. Comparison of mechanical properties of the scaffolds between LAM and LAMS processes

The stress-strain curves obtained from the static compression test are presented in Fig. 6. The static compression modulus was computed from the slope of the stress-strain curve at a strain level of 25%



**Fig. 6.** Static compression (stress-strain) curves of scaffolds fabricated using LAM and LAMS processes. (a) PU as the scaffold material; (b) CS as the scaffold material.

(Table 3), according to the testing standard ISO 7743 (Method 4). The trend of static moduli for the PU scaffolds was in agreement with the dynamic compression moduli, which are also summarized in Table 3. The tan values were in the range 0.3–0.5, indicating the elastomeric features of the PU scaffolds. For the CS scaffolds, the static compression moduli were slightly lower than the dynamic compression moduli, which are shown in Table 3. Low tan values were observed (0.1), indicating the fragile (weak plastic) nature of the CS scaffolds. This may also account for the greater dynamic moduli (compared with the static moduli) of the CS scaffolds.

The mechanical testing data revealed that the toughness of the PU scaffolds fabricated using different processes remained similar (overlapping stress-strain curves at higher strains), though the PU scaffolds fabricated through the LAMS process were even more flexible (with a lower modulus). In contrast, the CS scaffolds fabricated through the LAMS process were fairly stronger (with a greater modulus), probably due to the presence of inter-strand mesh structure in the CS-LAMS scaffolds. Overall, these data suggest that the LAMS process does not deteriorate the strength of scaffolds.

#### 3.5. Comparison of scaffold toxicity between LAM and LAMS processes

The LAM process does not affect normal cell growth and cellular differentiation in PU and CS scaffolds, as described in our previous studies

**Table 2**  
Comparison of strand diameters of PU and CS scaffolds between LAM and LAMS processes.

Scaffold material	Strand diameter ( $\mu\text{m}$ )		
	LAM		LAMS
	10 wt% EtOH	15 wt% EG	
PU	347 $\pm$ 2.89	391 $\pm$ 3.23 (+12.6%)	242 $\pm$ 6.25 (-30.3%)
CS	318 $\pm$ 8.05	242 $\pm$ 8.38 (-23.9%)	-

**Table 3**

Comparison of static compression moduli and dynamic compression properties (moduli and  $\tan\delta$ ) of PU and CS scaffolds between LAM and LAMS processes.

Scaffold material	Process	Support material (aq)	Static	Dynamic		
			Compression modulus (kPa)	Storage modulus ( $E'$ , kPa)	Loss modulus ( $E''$ , kPa)	$\tan\delta$
PU	LAM	–	31.3 ± 3.41	27.1 ± 2.92	13.7 ± 1.57	0.5 ± 0.0
	LAMS	10 wt% EtOH	17.1 ± 2.94	18.4 ± 2.83	9.8 ± 0.23	0.5 ± 0.1
	LAMS	15 wt% EG	21.0 ± 1.88	20.3 ± 2.29	5.2 ± 0.68	0.3 ± 0.0
	CS	–	3.5 ± 0.32	11.5 ± 2.86	1.1 ± 0.29	0.1 ± 0.0
CS	LAM	–	6.4 ± 1.36	22.9 ± 0.54	2.3 ± 0.31	0.1 ± 0.0
	LAMS	10 wt% EtOH				

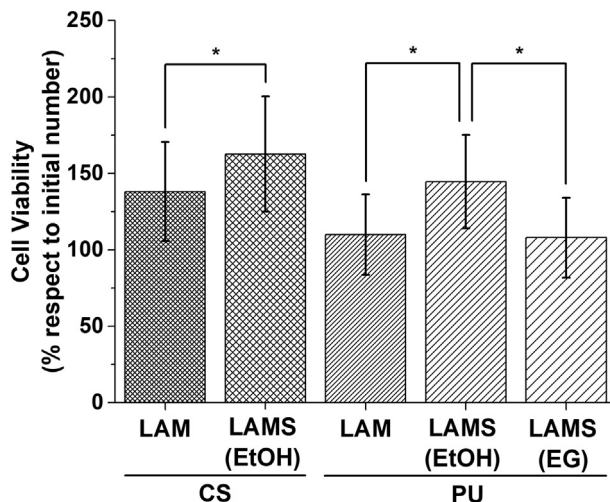


**Fig. 7.** Cell viability testing of PU and CS cylindrical scaffolds fabricated using LAM and LAMS processes with different support materials. The Cells employed in the test were MSCs and the culture time of the scaffolds was 24 h.

[18,22]. In the current study, the LAMS process was realized by integrating LAM with the proposed sacrificial process. To understand whether the proposed sacrificial process adversely affects cell growth, the viability of MSCs was evaluated by MTT assay. Fig. 7 illustrates the percentage of increase in the number of MSCs that were cultured for 24 h on the cylindrical scaffolds fabricated under varying manufacturing conditions. The cell number before seeding was set as 100%. The figure indicates that when the LAMS process was applied, the growth of MSCs was similar to or better than that with the LAM process, regardless of the material (i.e., PU or CS) used.

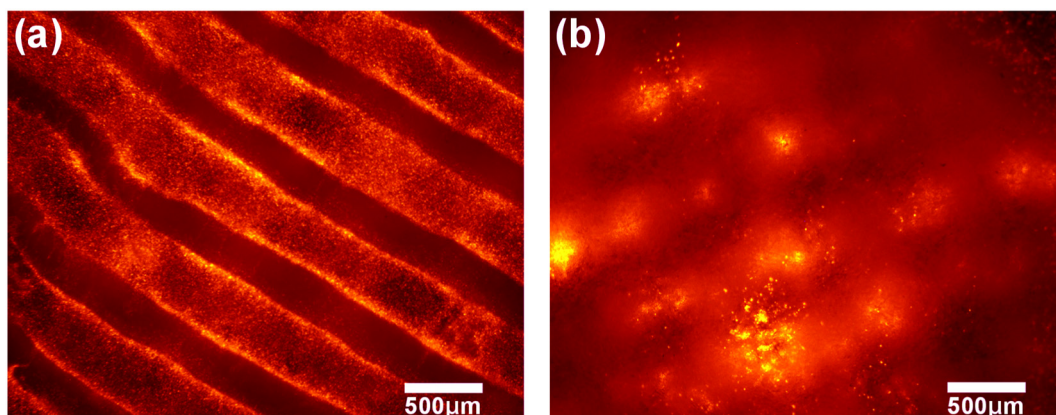
To demonstrate the distribution of cells on the scaffolds, thin cylindrical scaffolds (Fig. 2(b)) were fabricated using the LAM and LAMS processes, and cell labeling was then performed. Because of the opacity of

the PU ink, the amount of light penetrating the material was insufficient during image capturing and clear fluorescent images could not. Thus, only fluorescent images of the CS scaffolds fabricated through the LAM and LAMS processes were captured after the MSCs were seeded for 24 h and they are shown in Fig. 8.

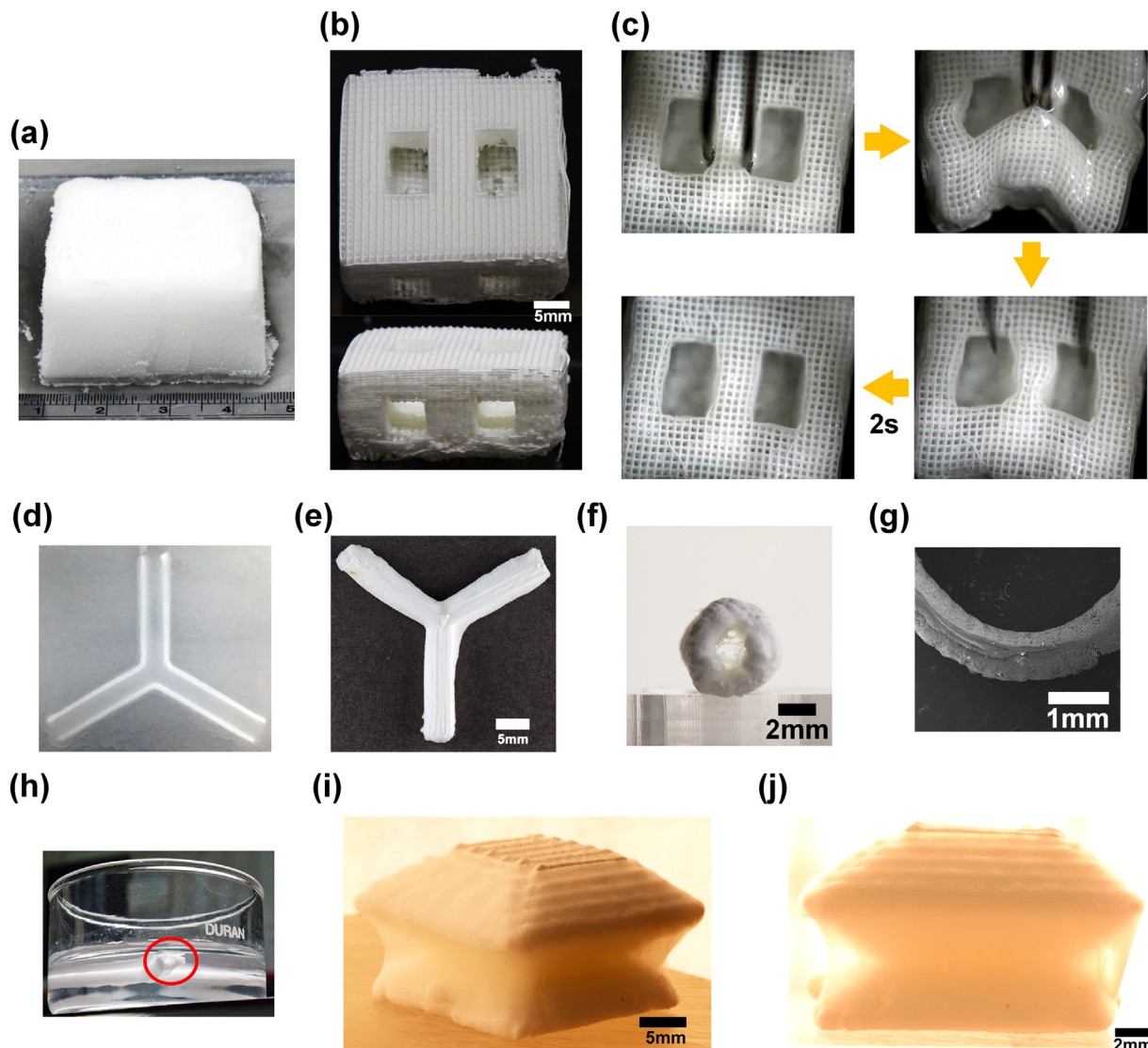
### 3.6. Successful fabrication of large scaffolds by the LAMS process with 10 wt % EtOH (aq) as the support material

Fig. 9 presents three complex scaffolds fabricated through the LAMS (EtOH) process. Except for the scaffolds in Fig. 9(g) and (h), which were fabricated from CS, all the scaffolds were fabricated from PU. Fig. 9(a) shows the unfinished product derived from the LAMS process. The PU scaffold was embedded in ice. Before the lyophilization process, the portion not embodying the scaffold could be resected in advance to accelerate the sublimation and evaporation of the support structure. Fig. 9(b) illustrates the finished product of the square scaffold after lyophilization, revealing micro- and nano-mesh structures clinging to the strands and pores of the scaffold. After immersion in DI water, the PEO reticular structure dissolved and the scaffold pores were clearly visible (Fig. 9(c)). When a pair of tweezers was used to grip the square scaffold and then release it, the scaffold recovered its original shape in approximately 2 s. This result confirms that the adhesion between the layers of the PU scaffold was firm and had elastic recovery capability. Therefore, the scaffold is potentially useful for soft tissue filling and TE in the future.

Because the proposed sacrificial process involves the sublimation of ice, the first square scaffold exhibited high porosity; hence, ice could easily evaporate from within the scaffold. To prove that this method is also applicable to scaffolds that have a smooth enclosed surface, we fabricated a Y-type tubular scaffold with a smooth shell. The tubular scaffold was embedded in ice during the fabrication process, and the split tube structure was clearly visible, as shown in Fig. 9(d) (where the white portion is the scaffold material and the other portion is the ice). Fig. 9(e) presents the finished product of the tubular scaffold after lyophilization. After cutting a branch of the Y-type tubular scaffold, a



**Fig. 8.** Cell labeling of CS cylindrical scaffolds: (a) fabricated using the LAM process; (b) fabricated using the LAMS process.



**Fig. 9.** Sample scaffolds fabricated using the LAMS (EtOH) process. (a) Square PU scaffold with dual inverted T-type inner channels embedded in ice after fabrication. (b) Top view and front view of the square PU scaffold after lyophilization. (c) After the square PU scaffold was immersed in DI water, the reticular structure dissolved, and an elastic recovery test was conducted to confirm the existence of sufficient adhesion between layers. (d) Y-type tubular PU scaffold embedded in ice during fabrication. (e) Top view of the tubular PU scaffold after lyophilization. (f) Front view of a branch of the tubular PU scaffold. (g) SEM image of the partial cross section of the tubular PU scaffold. (h) After the tubular PU scaffold was immersed in DI water, through-holes appeared. (i) Perspective view of the three-layer tapered CS scaffold. Reticular structures were observed inside and outside the CS scaffold. (j) Front view of the tapered CS scaffold.

through-hole with mesh structure was observed (Figure f). A piece of tubular scaffold was sliced by a knife for SEM examination (Figure g). The adhesion between layers was sufficient and the tubular scaffold did not fracture. After the tubular scaffold was immersed in DI water, the through-hole was seen (Fig. 9(h)).

Fig. 9(i) shows the three-layer tapered scaffold fabricated using CS, revealing that the scaffold was surrounded by a dense mesh structure. However, the mesh structure could be easily removed using scissors. The tapered scaffold was placed in front of high-intensity LED (light-emitting diode) light to capture perspective images in order to clearly observe the overall appearance of the scaffold, as shown in Fig. 9(j).

#### 4. Conclusions

In this study, we developed a spray-valve-based sacrificial process for LAM using simple water/ice as support materials. Two scaffold materials PU and CS with two support materials EtOH (aq), and EG (aq) were successfully employed to produce large and complex scaffolds. The

properties of the printed structures were adequately maintained and the adhesion between layers was sufficiently firm to resist elastic deformation. This study offers a framework for fabricating complex, suspended, and hollow structures in AM, particularly for extrusion-based methods, for not only biomedical but also industrial applications.

#### Author contributions

C.-Y. Liao designed the LAMS process. C.-Y. Liao and C.-S. Tseng designed the LAM process. W.-J. Wu and H.-C. Yang performed the experiments. C.-T. Hsieh synthesized the inks and performed cell viability assay and cell labeling. C.-Y. Liao and S.-h. Hsu wrote the manuscript.

#### Acknowledgements

This research is supported by Ministry of Science and Technology, Taiwan under Grant no. MOST 107-2218-E-002-026.

## References

- [1] R.D. Farahani, M. Dubé, D. Therriault, Three-dimensional printing of multifunctional nanocomposites: manufacturing techniques and applications, *Adv. Mater.* 28 (28) (2016) 5794–5821.
- [2] F.P.W. Melchels, M.A.N. Domingos, T.J. Klein, J. Malda, P.J. Bartolo, D.W. Hutmacher, Additive manufacturing of tissues and organs, *Prog. Polym. Sci.* 37 (8) (2012) 1079–1104.
- [3] X. Ren, H. Shao, T. Lin, H. Zheng, 3D gel-printing—an additive manufacturing method for producing complex shape parts, *Mater. Des.* 101 (2016) 80–87.
- [4] F. Liravi, E. Toyserkani, A hybrid additive manufacturing method for the fabrication of silicone bio-structures: 3D printing optimization and surface characterization, *Mater. Des.* 138 (2018) 46–61.
- [5] H. Li, C. Tan, L. L, Review of 3D printable hydrogels and constructs, *Mater. Des.* 159 (2018) 20–38.
- [6] H. Yoshimoto, Y.M. Shin, H. Terai, J.P. Vacanti, A biodegradable nanofiber scaffold by electrospinning and its potential for bone tissue engineering, *Biomaterials* 24 (12) (2003) 2077–2082.
- [7] Y. Jin, A. Compaan, T. Bhattacharjee, Y. Huang, Granular gel support-enabled extrusion of three-dimensional alginate and cellular structures, *Biofabrication* 8 (2) (2016), 025016..
- [8] J.S. Lee, J.M. Hong, J.W. Jung, J.H. Shim, J.H. Oh, D.W. Cho, 3D printing of composite tissue with complex shape applied to ear regeneration, *Biofabrication* 6 (2) (2014), 024103..
- [9] Z. Xiong, Y. Yan, S. Wang, R. Zhang, C. Zhang, Fabrication of porous scaffolds for bone tissue engineering via low-temperature deposition, *Scr. Mater.* 46 (11) (2002) 771–776.
- [10] L. Liu, Z. Xiong, Y. Yan, R. Zhang, X. Wang, L. Jin, Multinozzle low-temperature deposition system for construction of gradient tissue engineering scaffolds, *J. Biomed. Mater. Res. Appl. Biomater* 88 (1) (2009) 254–263.
- [11] G.H. Kim, S.H. Ahn, H. Yoon, Y.Y. Kim, W. Chun, A cryogenic direct-plotting system for fabrication of 3D collagen scaffolds for tissue engineering, *J. Mater. Chem.* 19 (2009) 8817–8823.
- [12] H. Kai, X. Wang, K.S. Madhukar, L. Qin, Y. Yan, R. Zhang, X. Wang, Fabrication of a two-level tumor bone repair biomaterial based on a rapid prototyping technique, *Biofabrication* 1 (2) (2009), 025003..
- [13] N.D. Doiphode, T. Huang, M.C. Leu, M.N. Rahaman, D.E. Day, Freeze extrusion fabrication of 13-93 bioactive glass scaffolds for bone repair, *J. Mater. Sci. Mater. Med.* 22 (3) (2011) 515–523.
- [14] C. Liu, Y. Li, L. Zhang, S. Mi, Y. Xu, W. Sun, Development of a novel low-temperature deposition machine using screw extrusion to fabricate poly(L-lactide-co-glycolide) acid scaffolds, *Proc. Inst. Mech. Eng. H* 228 (6) (2014) 593–606.
- [15] N. Munir, R.S. Larsen, A. Callanan, Fabrication of 3D cryo-printed scaffolds using low-temperature deposition manufacturing for cartilage tissue engineering, *Bioprinting* (2018)<https://doi.org/10.1016/j.bprint.2018.e00033>.
- [16] H.J. Yen, S.H. Hsu, C.S. Tseng, J.P. Huang, C.L. Tsai, Fabrication of precision scaffolds using liquid-frozen deposition manufacturing for cartilage tissue engineering, *Tissue Eng. Part A* 15 (5) (2009) 965–975.
- [17] B.C. Gross, J.L. Erkal, S.Y. Lockwood, C. Chen, D.M. Spence, Evaluation of 3D printing and its potential impact on biotechnology and the chemical sciences, *Anal. Chem.* 86 (7) (2014) 3240–3253.
- [18] K.C. Hung, C.S. Tseng, S.H. Hsu, Synthesis and 3D printing of biodegradable polyurethane elastomer by a water-based process for cartilage tissue engineering applications, *Adv. Healthc. Mater.* 3 (10) (2014) 1578–1587.
- [19] Y.J. Wang, U.S. Jeng, S.H. Hsu, Biodegradable water-based polyurethane shape memory elastomers for bone tissue engineering, *ACS Biomater. Sci. Eng.* 4 (4) (2018) 1397–1406.
- [20] L. Buruaga, H. Sardon, L. Irusta, A. González, M.J. Fernández-Berridi, J.J. Iruin, Electrospraying of waterborne polyurethanes, *J. Appl. Polym. Sci.* 115 (2) (2010) 1176–1179.
- [21] D. Eglin, M. Alini, Degradable polymeric materials for osteosynthesis: tutorial, *Eur. Cell. Mater.* 16 (2008) 80–91.
- [22] S.H. Hsu, C.H. Lin, C.S. Tseng, Air plasma treated chitosan fibers-stacked scaffolds, *Biofabrication* 4 (1) (2012), 015002..
- [23] C.T. Hsieh, C.Y. Liao, N.T. Dai, C.S. Tseng, B.L. Yen, S.H. Hsu, 3D printing of tubular scaffolds with elasticity and complex structure from multiple waterborne polyurethanes for tracheal tissue engineering, *Appl. Mater. Today* 12 (2018) 330–341.
- [24] H. Kim, G.H. Yang, C.H. Choi, Y.S. Cho, G. Kim, Gelatin/PVA scaffolds fabricated using a 3D-printing process employed with a low-temperature plate for hard tissue regeneration: fabrication and characterizations, *Int. J. Biol. Macromol.* 120 (Pt A) (2018) 119–127.
- [25] L. Liu, Z. Xiong, Y. Yan, R. Zhang, X. Wang, L. Jin, Multinozzle low-temperature deposition system for construction of gradient tissue engineering scaffolds, *J. Biomed. Mater. Res B Appl. Biomater* 88 (1) (2009) 254–263.
- [26] S. Ahn, H. Lee, E.J. Lee, G.H. Kim, A direct cell printing supplemented with low-temperature processing method for obtaining highly porous three-dimensional cell-laden scaffolds, *J. Mater. Chem. B* 2 (2014) 2773–2782.
- [27] D.B. Kolesky, R.L. Truby, A.S. Gladman, T.A. Busbee, K.A. Homan, J.A. Lewis, 3D bioprinting of vascularized, heterogeneous cell-laden tissue constructs, *Adv. Mater.* 26 (19) (2014) 3124–3130.
- [28] S. Pan, F. Sun, H. Shi, F. Zhang, X. Liu, W. Zhang, Evaluation of an immune-privileged scaffold for *in vivo* implantation of tissue-engineered trachea, *Biotechnol. Bioprocess Eng.* 19 (5) (2014) 925–934.
- [29] L. Utomo, M.M. Pleumeekers, L. Nimeskern, S. Nürnberg, K.S. Stok, F. Hildner, G.J. van Osch, Preparation and characterization of a decellularized cartilage scaffold for ear cartilage reconstruction, *Biomed. Mater.* 10 (1) (2015), 015010..
- [30] R. Landers, R. Mühlaupt, Desktop manufacturing of complex objects, prototypes and biomedical scaffolds by means of computer-assisted design combined with computer-guided 3D plotting of polymers and reactive oligomers, *Macromol. Mater. Eng.* 282 (1) (2000) 17–21.
- [31] A. Blaesi, D.F. Duarte Campos, M. Weber, S. Neuss, B. Theek, H. Fischer, W. Jähnen-Dechent, Biofabrication under fluorocarbon: a novel freeform fabrication technique to generate high aspect ratio tissue-engineered constructs, *Biores. Open Access* 2 (5) (2013) 374–384.
- [32] A.E. Jakus, S.L. Taylor, N.R. Geisendorfer, D.C. Dunand, R.N. Shah, Metallic architectures from 3D-printed powder-based liquid inks, *Adv. Funct. Mater.* 25 (45) (2015) 6985–6995.
- [33] B.Y. Ahn, D. Shoji, C.J. Hansen, E. Hong, D.C. Dunand, J.A. Lewis, Printed origami structures, *Adv. Mater.* 22 (20) (2010) 2251–2254.
- [34] A.S. Gladman, E.A. Matsumoto, R.G. Nuzzo, L. Mahadevan, J.A. Lewis, Biomimetic 4D printing, *Nat. Mater.* 15 (4) (2016) 413–418.
- [35] F.D. Bryant, M.C. Leu, Modeling and experimental results of concentration with support material in rapid freeze prototyping, *Rapid Prototyp. J.* 15 (5) (2009) 317–324.
- [36] M.C. Leu, D.A. Garcia, Development of freeze-form extrusion fabrication with use of sacrificial material, *J. Manuf. Sci. Eng.* 136 (6) (2014), 061014..
- [37] C.Y. Liao, W.J. Wu, C.T. Hsieh, C.S. Tseng, N.T. Dai, S.H. Hsu, Design and development of novel frozen-form additive manufacturing system for tissue engineering applications, *3D Print. Addit. Manuf.* 3 (4) (2016) 216–225.
- [38] J.Y. Jeng, J.C. Wang, T.T. Lin, Fast interior filling of model maker models using a spraying nozzle to accelerate build speed, *Rapid Prototyp. J.* 6 (4) (2000) 235–243.
- [39] P.J. Ho, M.L. Yen, J.D. Lin, L.S. Chen, H.I. Hu, C.K. Yeh, C.Y. Peng, C.Y. Lin, S.F. Yet, B.L. Yen, Endogenous KLF4 expression in human fetal endothelial cells allows for reprogramming to pluripotency with just OCT3/4 and SOX2—brief report, *Arterioscler. Thromb. Vasc. Biol.* 30 (10) (2010) 1905–1907.
- [40] M.L. Yen, C.H. Hou, K.Y. Peng, P.C. Tseng, S.S. Jiang, C.T. Shun, Y.C. Chen, M.L. Kuo, Efficient derivation and concise gene expression profiling of human embryonic stem cell-derived mesenchymal progenitors (EMPs), *Cell Transplant.* 20 (10) (2011) 1529–1545.
- [41] D.L. Teagarden, D.S. Baker, Practical aspects of lyophilization using non-aqueous co-solvent systems, *Eur. J. Pharm. Sci.* 15 (2) (2002) 115–133.
- [42] H. Seager, C.B. Taskis, M. Syrop, T.J. Lee, Structure of products prepared by freeze-drying solutions containing organic solvents, *J. Parenter. Sci. Technol.* 39 (4) (1985) 161–179.
- [43] K. Takaizumi, A curious phenomenon in the freezing-thawing process of aqueous ethanol solution, *J. Solut. Chem.* 34 (5) (2005) 597–612.
- [44] B. González, N. Calvar, E. Gómez, Á. Domínguez, Density, dynamic viscosity, and derived properties of binary mixtures of methanol or ethanol with water, ethyl acetate, and methyl acetate at  $T = (293.15, 298.15, \text{ and } 303.15)$  K, *J. Chem. Thermodyn.* 39 (12) (2007) 1578–1588.